

ORIGINAL ARTICLE

Open Access



# Extension of Flow Behaviour and Damage Models for Cast Iron Alloys with Strain Rate Effect

Chuang Liu<sup>1,2</sup>, Dongzhi Sun<sup>2\*</sup>, Xianfeng Zhang<sup>1\*</sup> , Florence Andrieux<sup>2</sup> and Tobias Gersterc<sup>3</sup>

## Abstract

Cast iron alloys with low production cost and quite good mechanical properties are widely used in the automotive industry. To study the mechanical behavior of a typical ductile cast iron (GJS-450) with nodular graphite, uni-axial quasi-static and dynamic tensile tests at strain rates of  $10^{-4}$ , 1, 10, 100, and  $250 \text{ s}^{-1}$  were carried out. In order to investigate the influence of stress state on the deformation and fracture parameters, specimens with various geometries were used in the experiments. Stress strain curves and fracture strains of the GJS-450 alloy in the strain rate range of  $10^{-4}$  to  $250 \text{ s}^{-1}$  were obtained. A strain rate-dependent plastic flow model was proposed to describe the mechanical behavior in the corresponding strain-rate range. The available damage model was extended to take the strain rate into account and calibrated based on the analysis of local fracture strains. Simulations with the proposed plastic flow model and the damage model were conducted to observe the deformation and fracture process. The results show that the strain rate has obviously nonlinear effects on the yield stress and fracture strain of GJS-450 alloys. The predictions with the proposed plastic flow and damage models at various strain rates agree well with the experimental results, which illustrates that the rate-dependent plastic flow and damage models can be used to describe the mechanical behavior of cast iron alloys at elevated strain rates. The proposed plastic flow and damage models can be used to describe the deformation and fracture analysis of materials with similar properties.

**Keywords** Dynamic behavior of materials, Strain rate dependency, Damage model, Voce model, Cast iron

## 1 Introduction

Cast iron with low production cost, excellent performance, low wear resistance, favourable vibration resistance and low gap sensitivity has become an important material in automotive industry. However, the cast iron

components are inevitably subjected to dynamic loading at work conditions such as impact accident or metal forming process, during which a wide range of loading situations (strains, strain rates and stress state) may occur. To predict the security performance of cast iron components in crash accident involving dynamic loading, it is necessary to determine the complex deformation and damage behavior of the cast iron by experiments. Particularly, describing the strain rate dependency with a flexible material model is required for simulations of dynamic behavior under complex loading conditions. Extensively, as strain-rate is an important factor in the plastic instability (necking) [1] and failure [2] of the metallic materials, investigation on the influence of strain rate on mechanical response including deformation and damage should be carried out.

\*Correspondence:

Dongzhi Sun  
[dong-zhi.sun@iwm.fraunhofer.de](mailto:dong-zhi.sun@iwm.fraunhofer.de)  
Xianfeng Zhang  
[lynx@njjust.edu.cn](mailto:lynx@njjust.edu.cn)

<sup>1</sup> School of Mechanical Engineering, Nanjing University of Science and Technology, Nanjing 210094, China

<sup>2</sup> Fraunhofer Institute for Mechanics of Materials (IWM), 79108 Freiburg, Germany

<sup>3</sup> Fraunhofer Institute for High Speed Dynamics, Ernst-Mach-Institute (EMI), 79104 Freiburg, Germany



© The Author(s) 2024. **Open Access** This article is licensed under a Creative Commons Attribution 4.0 International License, which permits use, sharing, adaptation, distribution and reproduction in any medium or format, as long as you give appropriate credit to the original author(s) and the source, provide a link to the Creative Commons licence, and indicate if changes were made. The images or other third party material in this article are included in the article's Creative Commons licence, unless indicated otherwise in a credit line to the material. If material is not included in the article's Creative Commons licence and your intended use is not permitted by statutory regulation or exceeds the permitted use, you will need to obtain permission directly from the copyright holder. To view a copy of this licence, visit <http://creativecommons.org/licenses/by/4.0/>.

Phenomenological plastic constitutive models, including Johnson-Cook (J-C) [3], Khan-Huang (K-H) [4], Khan-Huang-Liang (K-H-L) [5], Fields-Backofen (F-B) [6], Molinari-Ravichandran (M-R) [7], Voce-Kocks (V-K) [8, 9] and Arrhenius model [10], have been widely used in the simulation of metallic materials at high strain rates [11]. The J-C constitutive model are most widely used as a temperature, strain and strain rate dependent flow stress model, due to the simplicity and less requirement for material parameters. The success of application of J-C model in simulation results from the simplicity and requirement of less model parameters. Khan and Huang proposed a viscoplastic constitutive model to simulate the behavior of coarse-grained Al 1100 at a wide strain rate range [4]. Fields-Backofen proposed a simplified model with only three parameters to describe the strain sensitivity behaviour [6]. Molinari-Ravichandran model [7] is proposed based on a single internal variable, which has a better description for the flow behaviour of metals over a wide range of loading conditions. The Arrhenius equation [10] is widely used to describe the relationship between the strain-rate and flow stress at high temperatures. Voce proposed a constitutive model [8] for strain hardening, however, the formulation is strain rate and temperature insensitive.

As known to all, damage model is very important to describe the fracture characteristics of materials. Nowadays, damage models considering the effects of strain rate and stress state are beneficial for the crash simulation of automotive components. The failure strain can be defined as a function of the stress state (generally using the stress triaxiality and Lode parameter), the strain rate and the temperature. The damage models of Johnson-Cook (J-C) [12] and Bai-Wierzbicki (B-W) [13], for instance, are widely used in the crash simulations. The J-C damage model, a cumulative damage model, was proposed based on a series of tests with OFHC copper, Armco iron, and 4340 steel, which takes the effects of strain rate, temperature and stress triaxiality into account. However, the Lode parameter, the second parameter in addition to triaxiality to define the stress state completely, is not included in the J-C model. Recently, B-W model [14, 15] was proposed by combining the stress triaxiality with Lode parameter to achieve a better description of the damage characteristic [16, 17], which is validated by a series of experimental results. It explains well most experimental observations and is relatively easy to calibrate. For the damage model, fracture is postulated to occur when the accumulated equivalent plastic strain reaches a critical value which is a function of the stress state (stress triaxiality and Lode parameter) [18, 19]. This stress state dependent damage model was validated by Lee et al. [20], Bai et al. [21], Gilioli et al. [22], Sandburg et al. [23] and Habib et al. [24]

with experiments on different materials. However, B-W damage model ignores the effects of strain rate and temperature, which are important factors for the mechanical properties of metal materials. Based on the tensile experiments with temperature ranging from 200 °C to 480 °C, Amours et al. [25] extended the B-W damage model by taking the temperature into consideration, which was verified by relevant experimental results. Furthermore, the Gissmo damage model in the crash code LS-DYNA offers a possibility to define the failure strain as a function of triaxiality and Lode parameter in user mode through loading curves. Moreover, it is also possible to define a strain rate dependency model in a simple manner by giving a strain-rate dependent scaling factor.

In summary, for the application to cast iron materials, more attention should be paid to the following aspects: (1) Constitutive models with a better description of the effect of strain rate and temperature on flow stress should be investigated. (2) Damage model should be extended by taking stress state and strain rate into account. (3) Methods for determining the corresponding material damage parameters should be further investigated based on the experimental results.

In this paper, a systematic experimental investigation of GJS-450 cast iron with smooth, notched cylindrical and plane strain tensile specimens have been performed at the strain rates ranging from  $10^{-4}$  to  $250 \text{ s}^{-1}$ . A plastic flow law based on Voce model was proposed to describe the behaviour of GJS-450 at various strain rates. Deformation behaviour at different strain rates were observed and analyzed through simulation. The B-W damage model was extended by taking the interaction of strain rate and stress state into account. The modified strain rate dependent model was defined in the commercial finite element software LS/DYNA via its material card of add-erosion using the Gissmo option. Simulations of specimen tests at different stress states with different strain rates were conducted. The modified plastic flow model and damage models were validated by comparing the relevant experimental and numerical results.

## 2 Experimental Characterization of Strain-Rate Effects for Cast Iron Alloys

### 2.1 Tensile Tests on Different Specimens

The quasi-static and dynamic tensile tests on smooth cylindrical specimens with diameter of 4 mm and gauge length of 20 mm were performed with an electronic mechanical tensile machine, shown in Figure 1. The geometry of the smooth cylindrical tensile specimen is shown in Figure 2. Five strain rates,  $10^{-4}$ , 1, 10, 100 and  $250 \text{ s}^{-1}$ , were selected for the tensile experiments. The corresponding tensile velocities 0.002 mm/s, 24 mm/s, 240 mm/s, 2400 mm/s, 6000 mm/s were determined

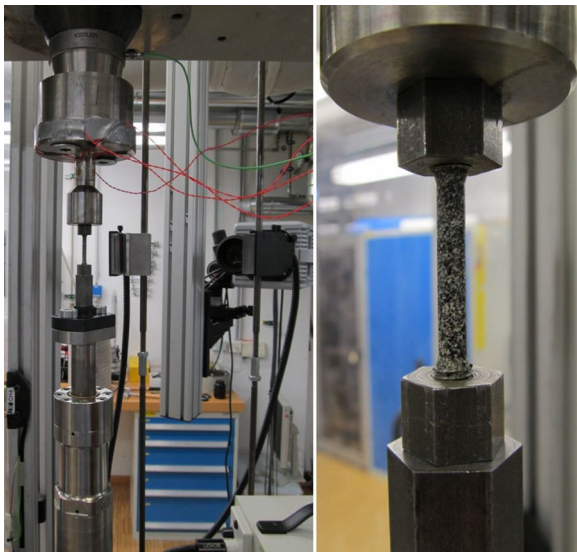


Figure 1 Setup of tensile tests

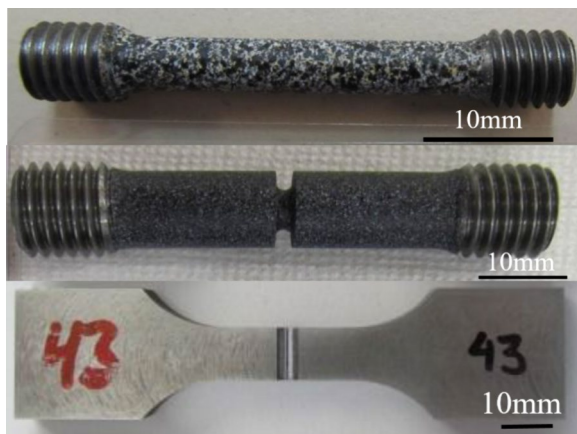


Figure 2 Geometry of tensile specimens

according to the strain rates and the gauge length of the specimens, respectively. The force was recorded by the load cell on the test machine, and the displacement was measured by the digital image correlation (DIC) and the extensometer. The engineering stress versus engineering strain curves for different strain rates were obtained.

### 2.2 Test Results and Discussions

The engineering stress versus strain curves of GJS-450 cast iron at strain rates  $10^{-4}$ , 1, 10, 100 and  $250 \text{ s}^{-1}$  are shown in Figure 3. The stress versus strain curves for notched specimens were shown in Figure 4 and Figure 5. As shown in Figure 3, 4 and 5, a significant strain rate hardening characteristic was indicated for the flow behavior of GJS-450 cast iron. The yield stresses at 0.2%

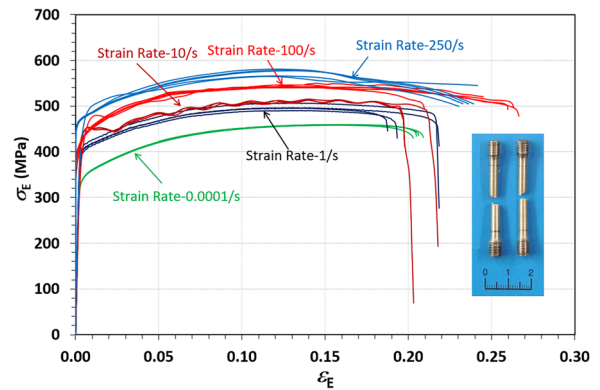


Figure 3 Experiment results at different strain rates for cylindrical specimens

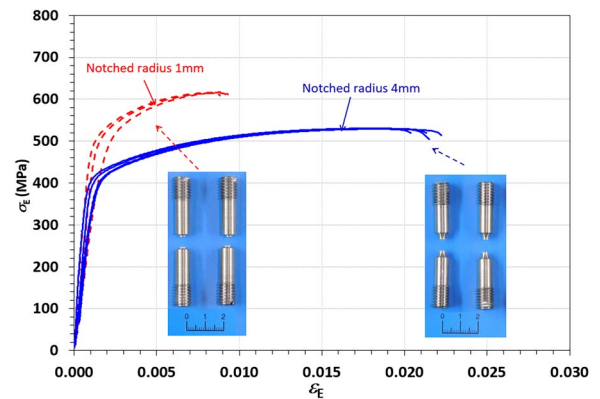


Figure 4 Experimental results for notched cylindrical specimens with tension velocity of 0.04 mm/s

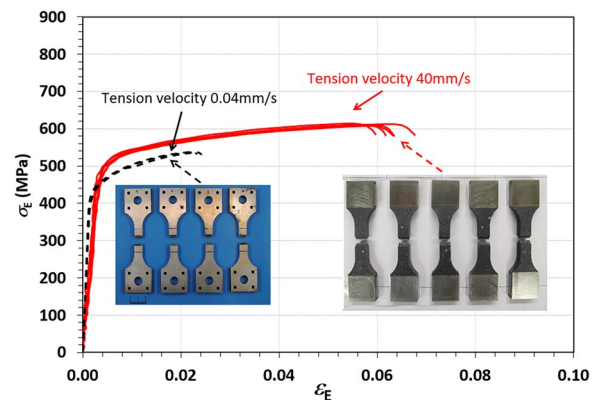
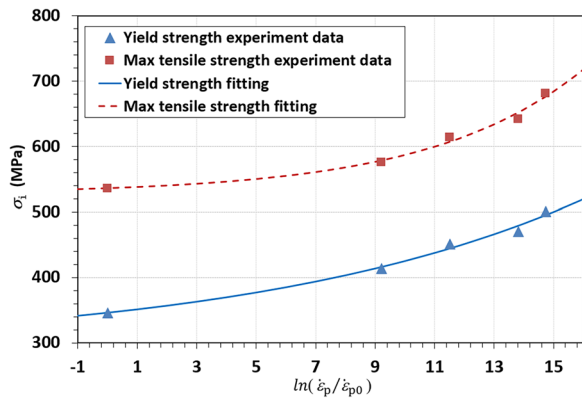
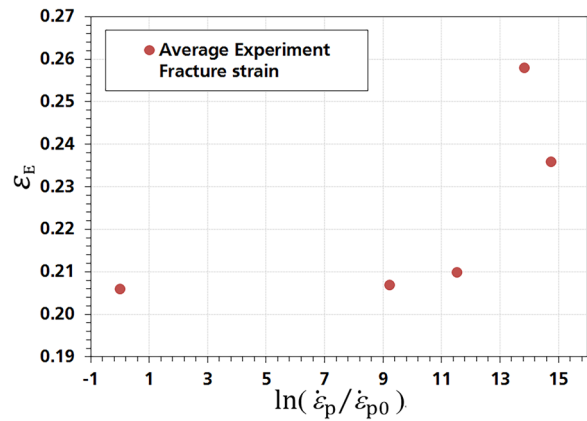


Figure 5 Experiment results for notched flat plate

plastic strain and ultimate tensile stresses at the different strain rates are reported in Figure 6. The normalized factor  $\ln(\dot{\epsilon}_p/\dot{\epsilon}_{p0})$  is defined by the reference plastic



**Figure 6** The yield stress and ultimate tensile strength at various strain rates



**Figure 7** Fracture strains at various strain rates

strain rate  $\dot{\epsilon}_{p0} = 10^{-4} \text{s}^{-1}$ . The dots in the figure are the experiment data.

According to the study of Yu et al. [26], the exponential law given by Eq. (1) was chosen to describe the strain-rate dependency of plastic flow stress:

$$f(\dot{\epsilon}_p) = C + D e^{n \ln(\dot{\epsilon}_p / \dot{\epsilon}_{p0})} \text{ or } f(\dot{\epsilon}_p) = C + D \left( \frac{\dot{\epsilon}_p}{\dot{\epsilon}_{p0}} \right)^n, \tag{1}$$

where  $C$  is the constant term,  $D$  is the linear coefficient,  $n$  is the exponential coefficient,  $f(\dot{\epsilon}_p)$  is the correction function,  $\dot{\epsilon}_p$  is the strain rate and  $\dot{\epsilon}_{p0}$  is the reference strain rate, here the  $\dot{\epsilon}_{p0}$  is taken as  $10^{-4} \text{s}^{-1}$ . The parameters are shown in Table 1. The yield stress at the strain rate  $\dot{\epsilon}_p$  is obtained:

$$\sigma(\dot{\epsilon}_p) = \sigma(\dot{\epsilon}_{p0}) \cdot f(\dot{\epsilon}_p), \tag{2}$$

where  $\sigma(\dot{\epsilon}_p)$  and  $\sigma(\dot{\epsilon}_{p0})$  are the yield stress with strain rate of  $\dot{\epsilon}_p$  and  $\dot{\epsilon}_{p0}$ .

Four or more specimens for each strain rate were conducted in the experiment. The average fracture strains under the different strain rates are obtained from the experimental curves, which are illustrated in Figure 7. Figure 7 shows that the fracture strain increases with the increasing strain rate. The strain rate effect on fracture strain is obviously nonlinear with the logarithmic

### 3 Deformation and Fracture Behaviour for Cast Iron Alloys

#### 3.1 Plastic Flow Law

J-C plastic flow law was proposed in 1983 [3], and was extensively used to describe the rate-dependent behavior

of various materials. The Johnson-Cook phenomenological equation, which contains four independent adjustable parameters (three of them are used to describe the static flow stress and one is to describe the strain rate effect), is widely used for high speed metal forming processes [27]. However, comparisons between the existing plastic flow models with the static experimental stress strain data [28, 29] showed that Voce [8] model has a better description of the flow behaviour for metallic materials. The good applicability of Voce model was also verified by experiment [30]. Here, a third-order Voce model is proposed to have a precise description of the static plastic flow characteristics. The static flow law is given by

$$\sigma(\dot{\epsilon}_{p0}) = Y_0 + \sum_{i=1}^3 A_i * (1 - \exp(-B_i * \epsilon^P)), \tag{3}$$

where  $\sigma(\dot{\epsilon}_{p0})$  is the flow stress,  $Y_0$  is the constant term,  $A_1, A_2, A_3, B_1, B_2, B_3$  are the material parameters, the parameters are shown in Table 1.

According to the results in Figure 6 and the discussion in Sect. 2.2, the correlation of the yield stress and the plastic strain rates can be described with an exponent function. Therefore, in order to describe the flow characteristic of cast iron, the Voce model is extended by taking strain rate into account by a multiplicative term given by

**Table 1** Parameters for the third order Voce flow law

$Y_0$ (MPa)	$A_1$ (MPa)	$A_2$ (MPa)	$A_3$ (MPa)	$B_1$
322.1	195.65	94.55	25.48	3.9
$B_2$	$B_3$	$C$	$D$	$n$
27.7	990	0.984	0.019	0.183

factor of strain rate.



Eq. (1). Then the plastic flow law at different strain rate is obtained and shown in Eq. (4).

The modified plastic flow law is defined as

$$\sigma = \left[ Y_0 + \sum_{i=1}^3 A_i * (1 - \exp(-B_i * \epsilon^p)) \right] \left( C + D e^{n \ln(\dot{\epsilon}_p / \dot{\epsilon}_{p0})} \right). \tag{4}$$

### 3.2 Material Models

#### 3.2.1 Deformation Model

For the simulation, two yield surfaces, the isotropy (MAT24 [31]) and anisotropy (MAT187 [32]) yield surfaces, were selected and applied in the FE code for the simulation via the commercial finite element software LS-DYNA. The isotropy yield criterion in MAT24, a classical yield criterion based on the Von Mises criterion, is widely used in the simulations of steel components. As an isotropic, strain-rate dependent elastic-plastic material model, it is possible for MAT24 to define the stress strain curves at different manner by users. A failure criterion was used in combination with MAT24. An isotropic yield surface is used in MAT187, and it is a strain-rate dependent elastic-plastic material model. The yield point of typical cast iron under tension is lower than under compression. For a better representation of material properties MAT187 was also applied. MAT187 uses separate stress-strain curves for compression, shear, uniaxial tension and bi-axial tension at different strain rates. Therefore, a lot of experimental investigations are necessary to

be conducted. The yield surface contains several regions defined by the four load curves as shown in Figure 8.

#### 3.2.2 Failure Model

The phenomenological Gissmo damage model, generalized incremental stress state dependant damage model, is proposed to describe the fracture process of the metallic material [33, 34]. A simplified input of material parameters is intended to consider the instability or localization, as it is a crucial issue in simulations. However, instead of using an exponential function to describe the relationship between failure strain and the reference strain rate, a more general piece-wise function is used to define failure strain by taking triaxiality and Lode parameter into consideration. Also, the strain rate dependency is generalized, instead of using the logarithmic function proposed in J-C model, a strain rate factor is defined for different strain rates. It should be noted that the rate factors in both J-C and Gissmo model are constants and independent on the stress triaxiality. Furthermore, the B-W model [13] was proposed by taking stress triaxiality and Lode parameter into account and was verified by experiment [35]. In the model, the locus for the failure strain at the reference strain rate is constructed in the 3D space of an equivalent fracture strain  $\epsilon_p$ , stress triaxiality  $\eta$ , and the Lode angle parameter  $\xi$ , using the following equation:

$$\epsilon_f(\eta, \xi) = \left[ \frac{1}{2} (D_1^- + D_1^+) - D_1^0 - D_2^0 \exp(-D_3^0 \eta) \right] \xi^2 + \left[ \frac{1}{2} (D_2^- \exp(-D_3^- \eta) + D_2^+ \exp(-D_3^+ \eta)) \right] \xi + \left[ \frac{1}{2} (D_1^+ - D_1^-) + \frac{1}{2} (D_2^+ \exp(-D_3^+ \eta) - D_2^- \exp(-D_3^- \eta)) \right] \xi + D_1^0 + D_2^0 \exp(-D_3^0 \eta), \tag{5}$$

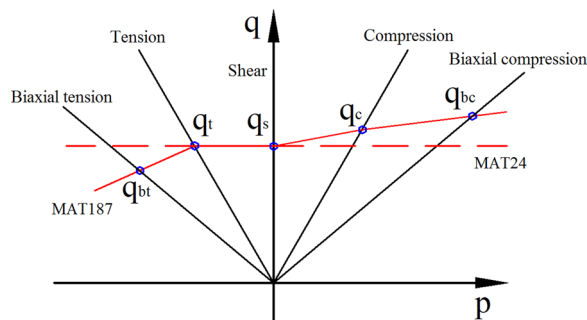


Figure 8 Normalized yield surfaces of two models

where  $\eta$  is the triaxiality of the specimen,  $\xi$  is the lode parameter of the specimen, the parameters of  $D_1^-$ ,  $D_1^+$ ,  $D_1^0$ ,  $D_2^-$ ,  $D_2^+$ ,  $D_2^0$ ,  $D_3^-$ ,  $D_3^+$  and  $D_3^0$  can be obtained from the experiments under different stress states.

Specifically, for the axisymmetric tension  $\xi=1$ , plane strain or generalized shear  $\xi=0$  and axisymmetric compression, e.g., biaxial tension  $\xi=-1$ , Eq. (5) is reduced to the form of J-C model:

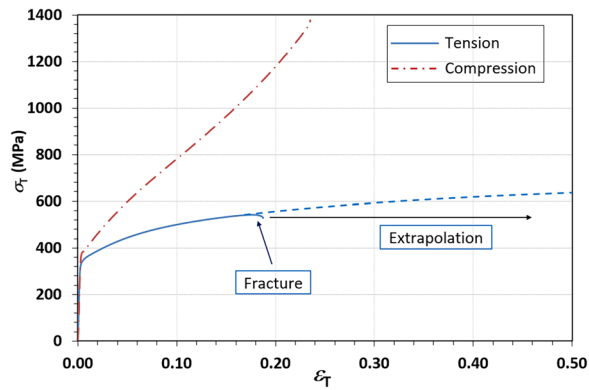


Figure 9 Flow behaviour of the cast iron material GJS 450 under uniaxial tension and compression

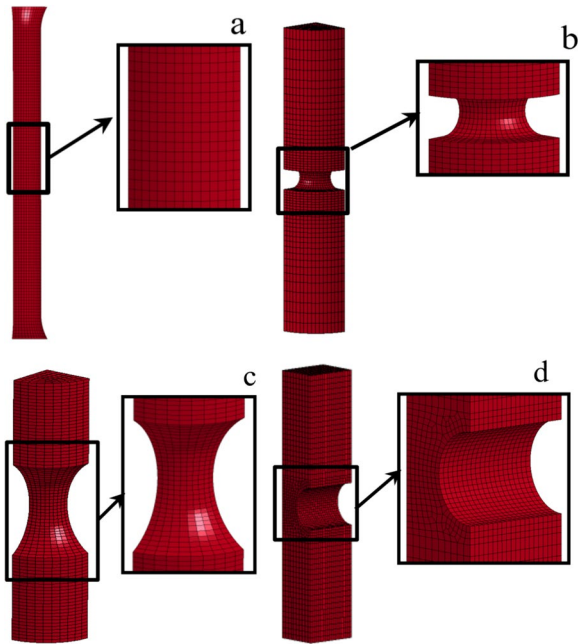


Figure 10 Models for simulations: (a) Smooth specimen, (b) Specimen with notch radius of 1 mm, (c) Specimen with notch radius of 4 mm, (d) Flat specimen with notch radius of 2 mm

$$\begin{aligned}
 \varepsilon_f(\eta, \xi = 1) &= D_1^+ + D_2^+ \exp(-D_3^+ \eta), \\
 \varepsilon_f(\eta, \xi = 0) &= D_1^0 + D_2^0 \exp(-D_3^0 \eta), \\
 \varepsilon_f(\eta, \xi = -1) &= D_1^- + D_2^- \exp(-D_3^- \eta).
 \end{aligned}
 \tag{6}$$

### 3.3 Deformation Behaviour of Cast Iron Alloys

For the cast iron, the yield stress under compression is larger than that under tension. Also, the hardening behaviours under tension and compression are different as shown in Figure 9. The reason is that the graphites

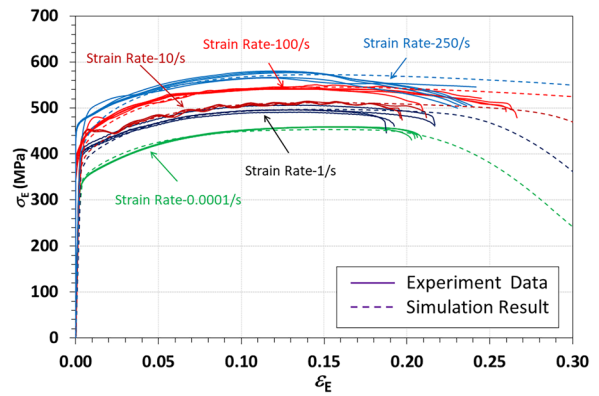


Figure 11 Experiment and simulation results for smooth tension

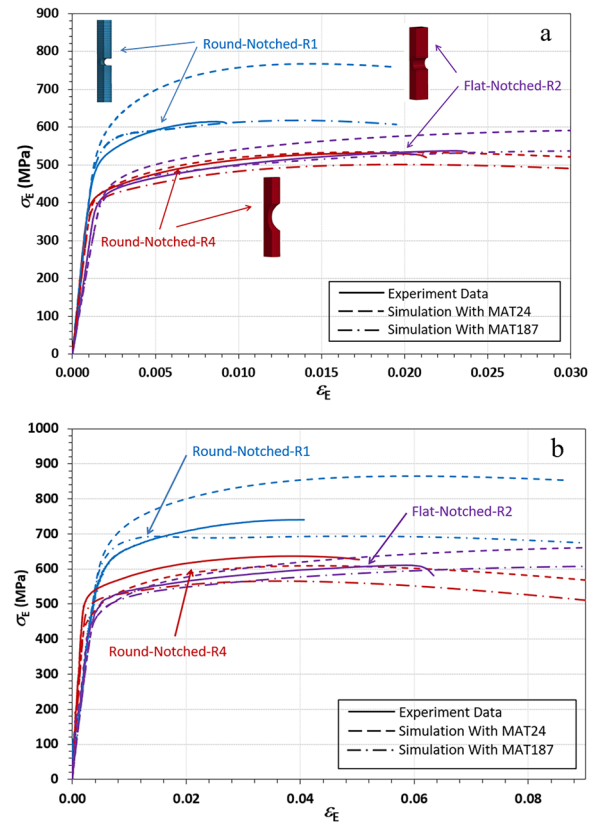


Figure 12 Simulation results with notched specimen: (a) Quasi-static load, (b) Dynamic load

separate from the matrix under tension and act as pores. However, the graphites can bear compressive loading together with the matrix. Material model 187 in LS-DYNA [33] provides a solution by introducing plastic flow curves under different stress states, which is shown in Figure 8. However, it requires much more experimental efforts to determine the stress strain curves under

biaxial and uniaxial compression, shear, biaxial and uniaxial tension. Thus, both material models MAT24 and MAT187 are used to compare their applicability for simulations of specimen tests firstly.

In order to verify the proposed rate-dependent plastic flow model, tensile tests on smooth cylindrical specimen, notched cylindrical specimen and notched flat plate were simulated. The new developed plastic flow model was applied with LS-DYNA via the flexible material model. To improve computational efficiency, a quarter of the models was established with an element size of 0.5 mm. Hexahedron solid elements with constant stress are used for the simulations. The models are shown in Figure 10.

The Von Mises criterion and the isotropy yield surfaces was applied in the simulations. The calculated engineering stress strain at five strain rates are compared with the experimental data, as shown in Figure 11. The numerical results at four strain rates are in excellent agreement with the experimental data. As shown in Figure 12, for the notched specimens, the simulation results with material model of MAT24 agree well with the experimental data under both quasi-static and dynamic loads, except the cylindrical specimen with notch radius of 1 mm. The main reason of discrepancy occurring in Figure 12 is that the same plastic flow curve is used in different stress state for MAT24. However, the plastic flow behaviour of GJS-450 cast iron are different under tension and compression. This characteristics accord with MAT187 in which different flow stress are adopted under different stress state.

It is obtained that the pressure dependent material model MAT187 is more applicable for GJS-450 cast iron according to the experimental results. It is shown in Figure 12(a) and Figure 12(b) that in the case of the specimen with notch radius of 1 mm, simulation results with MAT187 are in excellent agreement with experimental results. However, due to the interpolation between curves at different stress states and strain rates, the material model MAT187 works in a time-consuming way, which can result in inefficient calculations. Therefore, for the analysis of the damage process of cast iron, the material model of MAT24 is applied in the simulation.

### 3.4 Modelling of Fracture Behaviour

#### 3.4.1 Fracture Strains of Smooth Round Specimens

Deformation process of a smooth cylindrical specimen is shown in Figure 13. Local effective plastic strains versus global engineering strain in the specimen under strain rate of  $10^{-4} \text{ s}^{-1}$  are shown in Figure 14. Figure 13 and Figure 14 show that the local effective plastic strain  $\varepsilon_p$  and the global engineering strain  $\varepsilon$  are almost the same until the global engineering strain  $\varepsilon$  reaches 0.17.

When the global engineering strain exceeds 0.17, a strain gradient due to necking of the specimen occurs and a sharply increase in the local effective plastic strain  $\varepsilon_p$  can be observed. It can be found that the element near the center of the specimen has a larger plastic strain than that of the remaining part of element. Therefore, for the smooth cylindrical tensile specimen, the fracture occurs firstly near the central axis.

The evolution of the local plastic strain in the middle of the specimen and the global engineering strain for different strain rates are shown in Figure 15. As shown in Figure 14 and Figure 15, the local plastic strain  $\varepsilon_p$  linearly increases with the strain at the low engineering strain  $\varepsilon$  and a sharply increase occurs after the inflection point, while the inflection point of the curve increases with the strain rate. This means that an increase of strain rate results in a delay of onset of necking. Combining the experimental data of engineering fracture strain and the curves of local plastic strains versus engineering strains for different strain rates, the plastic fracture strains can be obtained, which are shown in Figure 16.

The local loading paths (plastic strain as function of triaxiality) in the specimen centre during the tensile process are obtained from the simulations which are shown in Figure 17. Taking the quasi-static tensile failure damage curve as reference and the function  $f(\dot{\varepsilon}, \eta)$  as modified parameter, fracture strains for different strain rate is obtained as Eq. (7):

$$\varepsilon_f(\eta, \xi, \dot{\varepsilon}) = \varepsilon_f(\eta, \xi, \dot{\varepsilon}_{p0}) * f(\dot{\varepsilon}, \eta), \quad (7)$$

where  $\varepsilon_f(\eta, \xi, \dot{\varepsilon}_{p0})$  is the fracture strain for quasi-static load,  $f(\dot{\varepsilon}, \eta)$  is the function for strain rate and triaxiality.

The values of function  $f(\dot{\varepsilon}, \eta)$  versus logarithmic strain rate are shown in Figure 18. Figure 18 reveals that the fracture strain no longer decreases linearly with the increase of logarithmic strain rate as assumed by the J-C model. Here, a secondary polynomial term is introduced to describe the strain rate effect.

$$f(\dot{\varepsilon}, \eta = 0.33) = E + F \ln(\dot{\varepsilon}_p / \dot{\varepsilon}_{p0}) + G (\ln(\dot{\varepsilon} / \dot{\varepsilon}_{p0}))^2, \quad (8)$$

where the parameters ( $E=1$ ,  $F=-0.067$ ,  $G=0.0029$ ) are obtained by combining the experimental data and simulation results.

In general, the local fracture strain decreases with increasing strain rate due to the earlier necking of the specimen at low strain rate. However, the local fracture strain increases slightly with the increase of strain rate in the region of strain rate greater than  $10 \text{ s}^{-1}$ , which is consistent with the model of Johnson-Cook at larger strain rates.

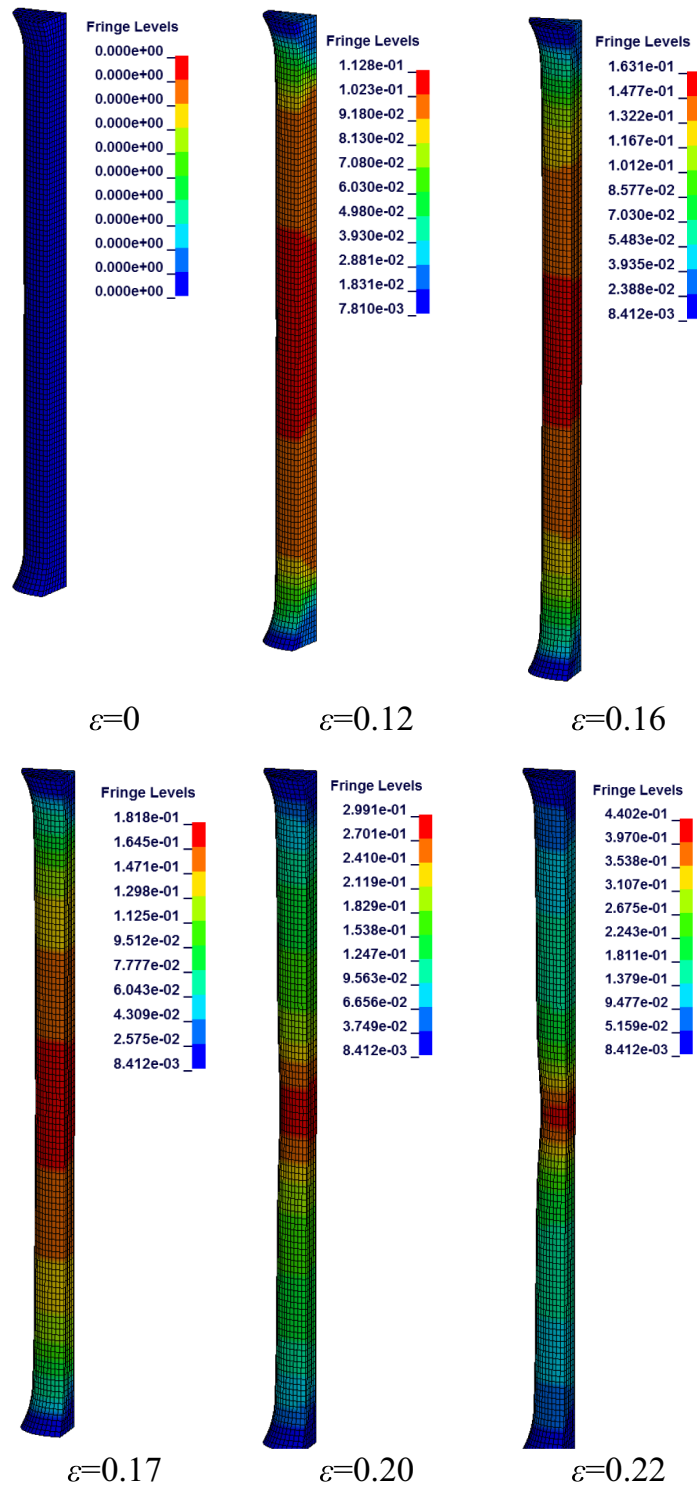


**Figure 13** Equivalent plastic strain distribution with increasing global engineering strain at strain rate  $10^{-4} s^{-1}$



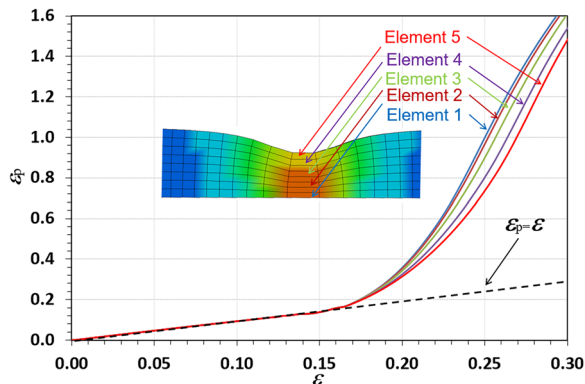


**Figure 14** Local plastic strain and engineering strain for strain rate  $10^{-4} \text{ s}^{-1}$

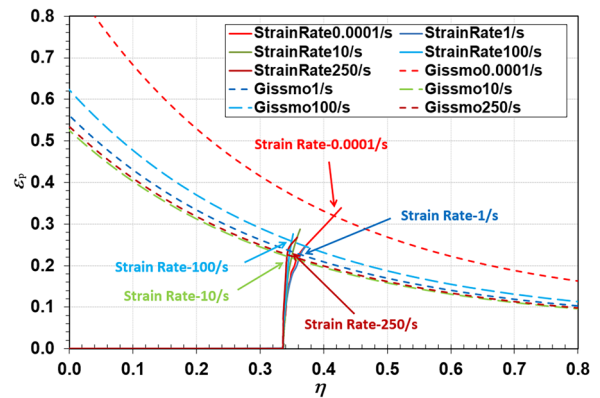


**Figure 17** Fitting failure strains under smooth tension at different strain rates

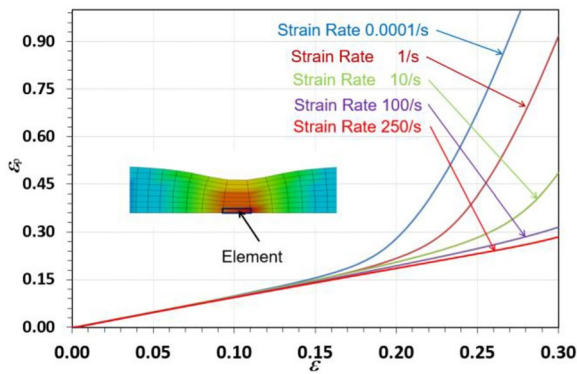


**Figure 15** Local plastic strain and engineering strain for different strain rates

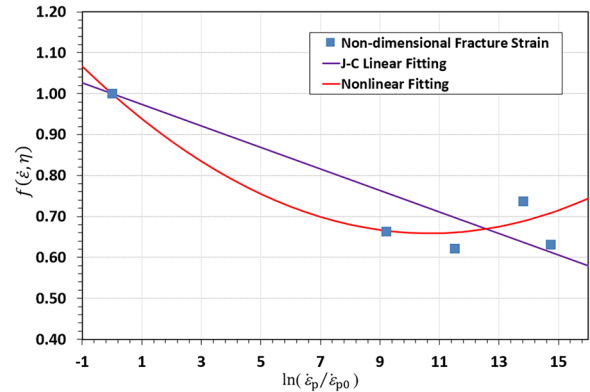


**Figure 18** Parameters for damage model at different strain rates

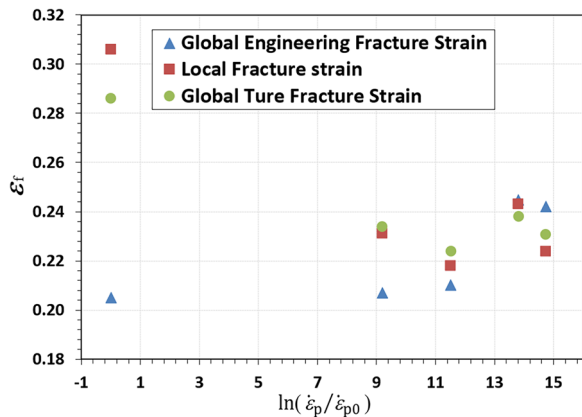


**Figure 16** Fracture strains at different strain rates

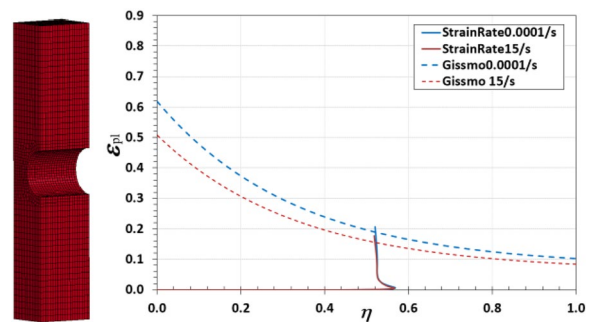


**Figure 19** Fitting damage curve for notched flat plate

### 3.4.2 Fracture Strains of Notched Specimens

To investigate the effect of the triaxiality on fracture strain, analysis of tests on flat plane with notch radius of 2 mm (plane strain specimen) and cylindrical specimens

with notch radius of 1 mm and 4 mm are performed in a similar way as described in Section 3.4.1. The Von Mises criterion and the isotropy yield surfaces was applied in the simulations. The parameters for the modified damage model are obtained by inverse simulation of all specimen tests. It is shown in Figures 19, 20 and 21 that the influence of strain rate on failure strain is different under different triaxialities.

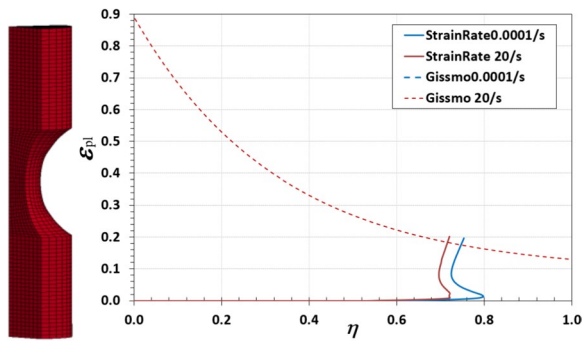


**Figure 20** Fitting damage curve for cylindrical specimens with a notch radius of 4 mm

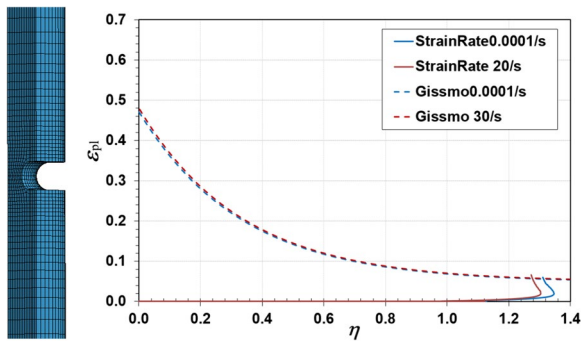


**Figure 21** Fitting Gissmo damage curve for cylindrical specimens with a notch radius of 1 mm

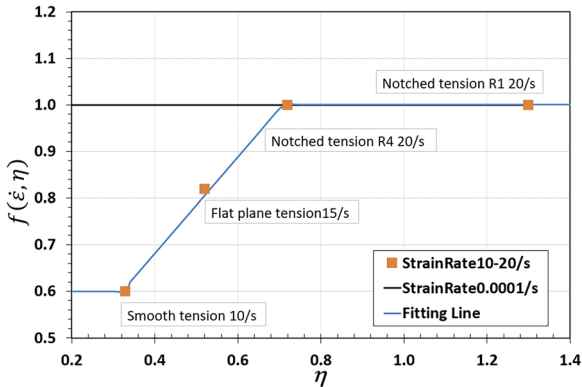


**Figure 22** Factor of strain rate depending on failure strain for different triaxialities

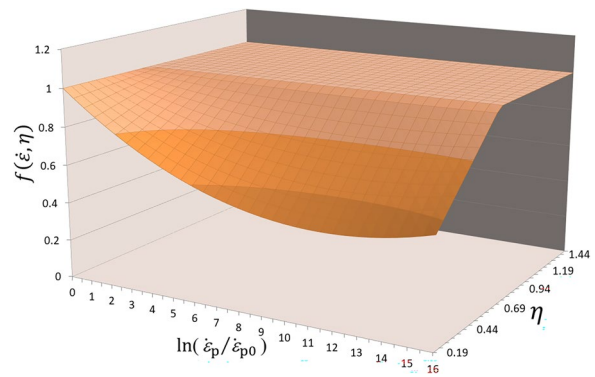


**Figure 23** The modified damage surface at different strain rate

Figure 22 illustrates that the strain rate factor for failure  $f(\dot{\epsilon}, \eta)$  shows a linear increasing trend with the triaxiality, then turns to a stable value if the small difference between  $10 \text{ s}^{-1}$ ,  $15 \text{ s}^{-1}$  and  $20 \text{ s}^{-1}$  in strain rate is ignored. Accordingly, the function for strain rate dependency for different triaxialities can be written as:

$$f(\dot{\epsilon} = 10, \eta) = \begin{cases} 0.6, & \eta \leq 0.33, \\ n * \eta + m, & 0.33 < \eta < 0.72, \\ 1, & \eta \geq 0.72, \end{cases} \quad (9)$$

where  $m$  is the constant term,  $n$  is the linear coefficient,  $m=0.27$  and  $n=1.03$  can be obtained by fitting the determined failure strains at strain rate of  $10/\text{s}$  and quasi-static loading.

## 4 Fracture Behaviour of Cast Iron Alloys with Modified Damage Model

### 4.1 Modified Damage Model

Based on the analysis above, it is plausible that  $\epsilon_f$  is not constant under different loading conditions, which is consistent with previous study [36]. The fracture strain of cast iron GJS-450 is sensitive to strain rates and triaxiality. Combining Eq. (5) and Eq. (7), a modified function  $f(\dot{\epsilon}, \eta)$  is proposed in order to take the coupling effect of strain rate and triaxiality into account. The strain rate dependent fracture strain can be written as

$$\epsilon_f(\eta, \xi, \dot{\epsilon}) = \left\{ \begin{aligned} & \left[ \frac{1}{2}(D_1^- + D_1^+) - D_1^0 - D_2^0 \exp(-D_3^0 \eta) \right] \xi^2 \\ & + \left[ \frac{1}{2}(D_2^- \exp(-D_3^- \eta) + D_2^+ \exp(-D_3^+ \eta)) \right] \xi \\ & + D_1^0 + D_2^0 \exp(-D_3^0 \eta) \end{aligned} \right\} * f(\dot{\epsilon}, \eta). \quad (10)$$

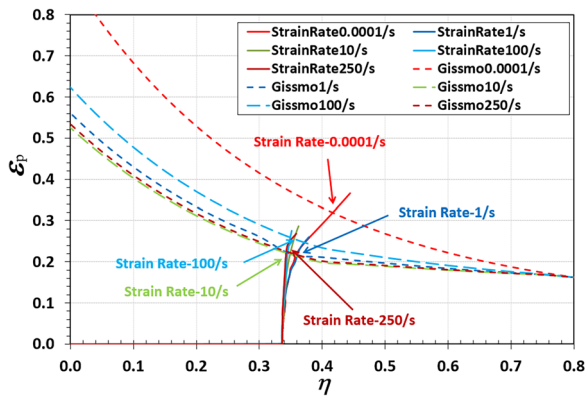


**Figure 24** The modified damage curves for smooth tension at different strain rate

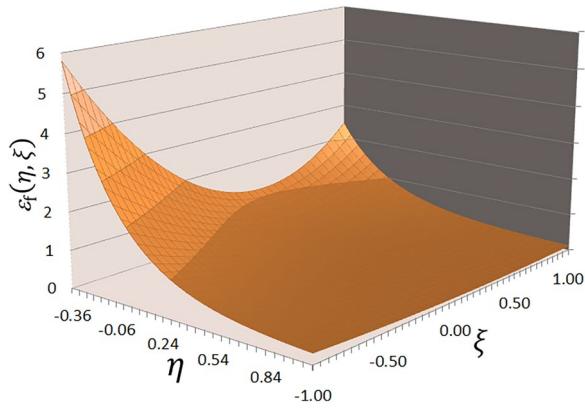


**Figure 25** Damage surface for strain rate 0.0001/s

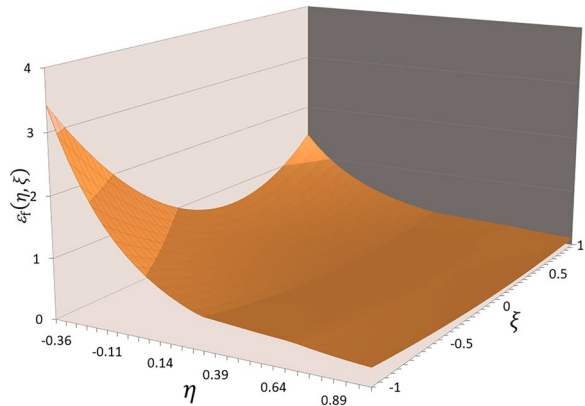


**Figure 26** Damage surface for strain rate 10/s

The parameters are taken as  $D_1^- = 0.2$ ,  $D_1^+ = 0.09$ ,  $D_1^0 = 0.08$ ,  $D_2^- = 1.9$ ,  $D_2^+ = 0.8$ ,  $D_2^0 = 0.45$ ,  $D_3^- = 3$ ,  $D_3^+ = 3$ ,  $D_3^0 = 3$ , which are taken from the study of Sun et al. [37].

It is assumed that the effect of strain rate and triaxiality on the fracture strain  $f(\dot{\epsilon}, \eta)$  is continuous. Besides,

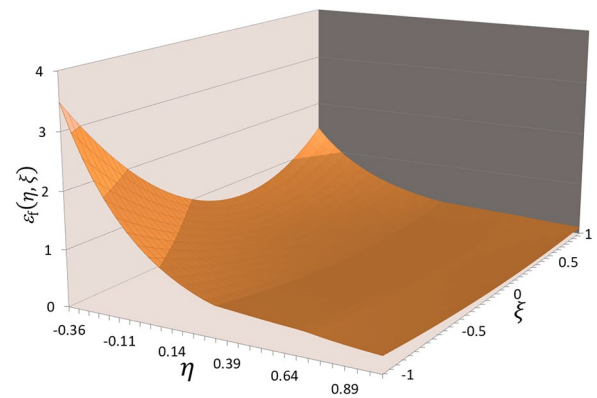


**Figure 27** Damage surface for strain rate 250/s

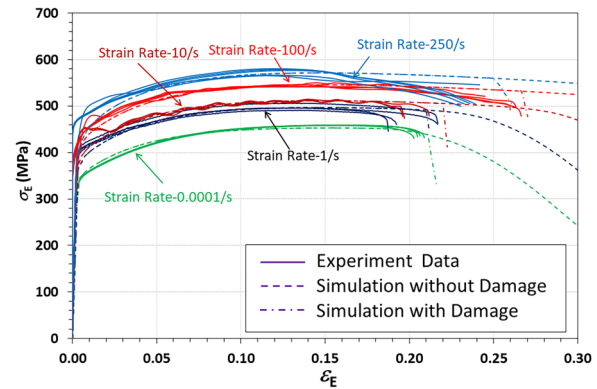


**Figure 28** Comparison of experiment and simulation for smooth tension

$f(\dot{\epsilon} = 0.0001, \eta) = 1$ ,  $f(\dot{\epsilon}, \eta > 0.72) = 1$  and Eq. (8), Eq. (9) are taken as the boundary conditions for the function. According to the method of spatial stereo geometry, the function  $f(\dot{\epsilon}, \eta)$  can be defined as

$$f(\dot{\epsilon}, \eta) = [1 - E - F \ln(\dot{\epsilon}_p / \dot{\epsilon}_{p0}) - G(\ln(\dot{\epsilon}_p / \dot{\epsilon}_{p0}))^2] * (\eta - H) / I + 1, \tag{11}$$

where  $E$  is the constant term,  $F$  is the linear coefficient,  $G$  is quadratic coefficient, the parameters are taken as  $E=1$ ,  $F=-0.067$ ,  $G=0.0029$ ,  $H=0.72$ ,  $I=0.39$ .

According to Eq. (11), the surface for function  $f(\dot{\epsilon}, \eta)$  is obtained, which is shown in Figure 23.

Combining Eq. (10) and Eq. (11), the damage surface for different strain rate and the damage curves for GJS-450 at different strain rate are obtained, which are shown in Figures 24, 25, 26 and 27.

#### 4.2 Simulation with the Modified Damage Model

In order to verify the new rate-dependent damage model, simulations of tension tests on smooth cylindrical

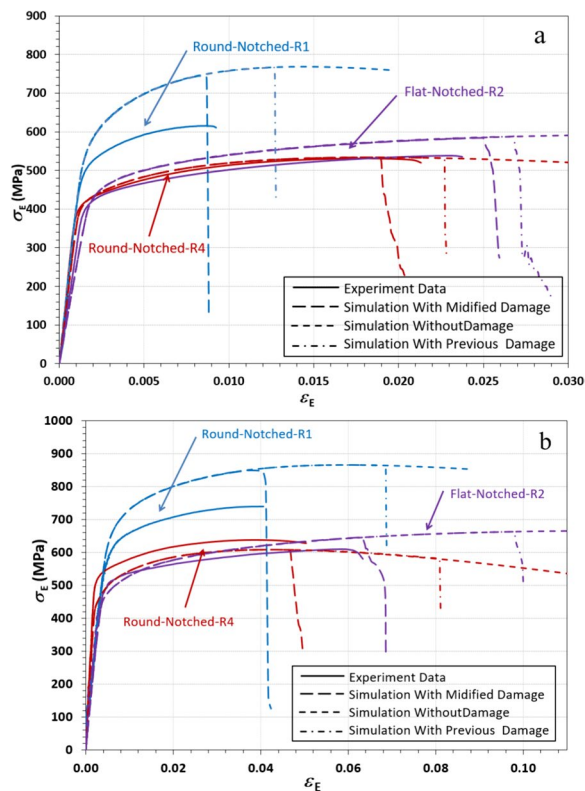


**Figure 29** Comparison of experiment and simulation for notched tension: (a) Quasi-static loading, (b) Dynamic loading

specimen, notched cylindrical specimen and notched flat plate (plane strain) were conducted. The new modified damage model was realized with the commercial finite element software LS-DYNA. The Von Mises criterion and the isotropy yield surfaces was applied in the simulations to study the fracture behaviour of cast iron alloys which related to Figures 28, 29.

Simulation results with the modified Gissmo damage model in combination with MAT24 for smooth tensile specimens at different strain rates are shown in Figure 29. It shows that the fracture strains at different strain rates are in excellent agreement with the experimental data. Moreover, simulation results with the proposed damage model and previous model for notched specimens under quasi-static load and dynamic load are shown in Figure 29(a) and Figure 29(b), respectively. As is shown in Figure 29, the proposed damage model has a better description for the fracture behaviour of the specimen compared with the previous damage model. The calculated fracture strains of round notched specimens (R1, R4) and flat-notched specimens R2 with the proposed damage model agree well with the corresponding experimental results, which indicates that the modified damage model has a good description of the damage characteristics of GJS-450 at different strain rates.

## 5 Conclusions

Quasi-static and dynamic tensile experiments for GJS-450 cast iron at strain rates ranging from  $10^{-4}$  to  $250 \text{ s}^{-1}$  were performed on smooth and notched specimens with radius of 1 mm and 4 mm, respectively. A significant strain rate dependent mechanical behaviour was observed during deformation and failure deformation process. A strain rate dependent plastic flow law based on Voce model and a damage model by taking strain rate, triaxiality and stress state into account were proposed to describe the mechanical behaviour of GJS-450 at different strain rates. Simulations on different specimen tests were conducted to verify the validity of the proposed models. The main conclusions are as follows:

- (1) The yield strength and damage characteristics of GJS-450 cast iron have an obvious relationship with strain rates.
- (2) Based on the experimental results, the Voce model is extended to describe strain-rate dependency of plastic flow behaviour. Simulation results with modified plastic flow law agree well with the experimental results. The modified plastic flow model can be used to describe the mechanical behaviour of GJS-450 cast iron.
- (3) The strain rate and stress state dependent damage model was proposed to describe the mechanical behaviour of GJS-450 at different strain rates. The calculated fracture strains with the new developed strain-rate dependent damage model agrees well with the experimental results. The extended rate dependent damage model can be used to describe the damage behaviour of GJS-450 cast iron.

## Acknowledgements

Not applicable.

## Authors' Contributions

XZ and DS were in charge of the whole trial; CL wrote the manuscript; FA and TG assisted with sampling and laboratory analyses. All authors read and approved the final manuscript.

## Funding

Supported by National Natural Science Foundation of China (Grant Nos.12202205, U1730101), the Federal Ministry of Economic Affairs and Energy (BMWi) via the German Federation of Industrial Research Associations 'Otto von Guericke' e.V. (AiF) (IGF-Nr. 19567N) and Forschungsvereinigung Automobiltechnik e.V. (FAT).

## Data availability

Data, models, or code that support the findings of this study are available from the corresponding author upon reasonable request.

## Declarations

### Competing Interests

The authors declare that they do not have any commercial or associative interest that represents a conflict of interest in connection with the work submitted.

Received: 31 October 2023 Revised: 31 October 2023 Accepted: 8 May 2024

Published online: 08 July 2024

## References

- [1] C Koomson, S E Zeltmann, N Gupta. Strain rate sensitivity of polycarbonate and vinyl ester from dynamic mechanical analysis experiments. *Advanced Composites and Hybrid Materials*, 2018, 1: 341–346.
- [2] A Trondl, D Z Sun, F Andrieux. Simulation of deformation and failure behavior of high strength steels for crash-loading scenarios. *The 5th International Conference on Steel in Cars and Trucks*, Amsterdam-Schiphol, 2017.
- [3] Y Zhang, J C Outeirob, T Mabroukic. On the selection of Johnson-cook constitutive model parameters for Ti-6Al-4V using three types of numerical models of orthogonal cutting. *The 15th CIRP Conference on Modelling of Machining Operations*, 2015, 31: 112–117.
- [4] A S Khan, S Hlang. Experimental and theoretical study of mechanical behavior of 1100 aluminum in the strain rate range  $10^{-5}$ – $10^4$ s $^{-1}$ . *International Journal of Plasticity*, 1992, 8(4): 397–424.
- [5] B Farrokh, A S Khan. Grain size, strain rate, and temperature dependence of flow stress in ultra-fine grained and nanocrystalline Cu and Al: synthesis, experiment, and constitutive modeling. *International Journal of Plasticity*, 2009, 25(5): 715–732.
- [6] R Ferreira, E Silva, C Nascimento, et al. Thermomechanical behavior modeling of a Cr-Ni-Mo-Mn-N austenitic stainless steel. *Materials Sciences and Applications*, 2016, 7: 803–822.
- [7] N Yan, Z Li, Y B Xu, et al. Shear localization in metallic materials at high strain rates. *Progress in Materials Science*, 2021, 119: 1–89.
- [8] G Sainath, B K Choudhary, J Christopher, et al. Applicability of Voce equation for tensile flow and work hardening behaviour of P92 ferritic steel. *International Journal of Pressure Vessels and Piping*, 2015, 132–133: 1–9.
- [9] Q Rong, Z S Shi, Y Li, et al. Constitutive modelling and its application to stress-relaxation age forming of AA6082 with elastic and plastic loadings. *Journal of Materials Processing Technology*, 2021, 295: 1–12.
- [10] S B Aziz, T J Woo, M F Kadir, et al. A conceptual review on polymer electrolytes and ion transport models. *Journal of Science: Advanced Materials and Devices*, 2018, 3(1): 1–17.
- [11] A R Khalifeh, A D Banaraki, H D Manesh, et al. Investigating of the tensile mechanical properties of structural steels at high strain rates. *Materials Science and Engineering: A*, 2018, 712: 232–239.
- [12] X Wang, J Shi. Validation of Johnson-Cook plasticity and damage model using impact experiment. *International Journal of Impact Engineering*, 2013, 60: 67–75.
- [13] Y L Bai, T Wierzbicki. A new model of metal plasticity and fracture with pressure and Lode dependence. *International Journal of Plasticity*, 2008, 24(6): 1071–1096.
- [14] Y Guo, Y Xie, D Wang, et al. An improved damage-coupled viscoplastic model for predicting ductile fracture in aluminum alloy at high temperatures. *Journal of Materials Processing Technology*, 2021, 296: 1–13.
- [15] P Zhu, Q Zhang, H Xu, et al. Experimental and numerical investigation on plasticity and fracture behaviors of aluminum alloy 6061-T6 extrusions. *Archives of Civil and Mechanical Engineering*, 2021, 12: 1–15.
- [16] A Keshavarz, R Ghajar, G Mirone. A new experimental failure model based on triaxiality factor and Lode angle for X-100 pipeline steel. *International Journal of Mechanical Sciences*, 2014, 80: 175–182.
- [17] B Jia, A Rusinek, R Pesci, et al. Simple shear behavior and constitutive modeling of 304 stainless steel over a wide range of strain rates and temperatures. *Procedia Manufacturing*, 2021, 154: 1–14.
- [18] J Gao, T He, Y Huo, et al. Comparison of modified Mohr–Coulomb model and Bai–Wierzbicki model for constructing 3D ductile fracture envelope of AA6063. *Chinese Journal of Mechanical Engineering*, 2021, 34: 35.
- [19] Y Jia, Y L Bai. Ductile fracture prediction for metal sheets using all-strain-based anisotropic eMMC model. *International Journal of Mechanical Sciences*, 2016, 115: 516–531.
- [20] S Lee, J Lee, J Song, et al. Fracture simulation of cold roll forming process for aluminum 7075-T6 automotive bumper beam using GISSMO damage model. *Progress in Natural Science: Materials International*, 2018, 15: 751–758.
- [21] Y L Bai, T Wierzbicki. Application of extended Mohr–Coulomb criterion to ductile fracture. *International Journal of Fracture*, 2010, 161(1): 1–20.
- [22] A Gilioli, A Manesa, M Giglio, et al. Predicting ballistic impact failure of aluminium 6061-T6 with the rate-independent Bao Wierzbicki fracture model. *International Journal of Impact Engineering*, 2015, 76: 207–220.
- [23] H Sandberg, O Rydholm. Evaluation of material models to predict material failure in LS-DYNA. *TFHF*, 5209, 2016.
- [24] S A Habib, J T Lloyd, C S Meredith, et al. Fracture of an anisotropic rare-earth-containing magnesium alloy (ZEK100) at different stress states and strain rates: Experiments and modelling. *International Journal of Plasticity*, 2019, 122: 285–318.
- [25] D G Amours, A Ilinich. High temperature characterization and material model calibration for hot stamping of AA7075 aluminium sheet. *IOP Conference Series: Materials Science and Engineering*, 2018, 418(1).
- [26] H Yu, Y Guo, X Lai. Rate-dependent behavior and constitutive model of DP600 steel at strain rate from  $10^{-4}$  to  $10^3$  s $^{-1}$ . *Materials and Design*, 2009, 30(7): 2501–2505.
- [27] J D Bressan, K Lopez. New constitutive equation for plasticity in high speed torsion tests of metals. *International Journal of Material Forming*, 2008, 1(1): 213–216.
- [28] M Zhang, J Li, B Tang, et al. Mechanical characterization and strain-rate sensitivity measurement of Ti-7333 alloy based on nanoindentation and crystal plasticity modeling. *Progress in Natural Science: Materials International*, 2018, 28: 718–723.
- [29] Q Jia, Y Wang, R Mei, et al. The dependences of deformation temperature on the strain-hardening characteristics and fracture behavior of Mn–N bearing lean duplex stainless steel. *Materials Science and Engineering A*, 2021, 819: 1–12.
- [30] Z Xu, L Peng, M K Jain, et al. Local and global tensile deformation behavior of AA7075 sheet material at 673K and different strain rates. *International Journal of Mechanical Sciences*, 2021, 195: 1–16.
- [31] S A Irfan, R Razali, K KuShaari, et al. A review of mathematical modeling and simulation of controlled-release fertilizers. *Journal of Controlled Release*, 2018, 271: 45–54.
- [32] F Karlsson, W Gradin. *Modelling and simulation of composites crash tests for validation of material models using LS-DYNA*. Chalmers University of Technology, 2016: 1–79.
- [33] M Kumar, U Deep, P M Dixt. Simulation and analysis of ballistic impact using continuum damage mechanics (CDM) model. *Procedia Engineering*, 2017, 173: 190–197.
- [34] F Neukamm, M Feucht, A Haufe. *Considering damage history in crashworthiness simulations*. Ls-Dyna Anwenderforum, 2009.
- [35] D Mariaa, I Kerimb, C Till, et al. Material characterization and validation studies for modeling ductile damage during deep drawing. *Procedia Engineering*, 2017, 183: 77–82.
- [36] S R Hiremath, D Alapur, D R Mahapatra. Stress triaxiality in damage models. *Springer Transactions in Civil and Environmental Engineering*, 2017: 247–264.
- [37] D Z Sun, F Andrieux, C Fehrenbach. *Crash simulation of cast iron alloys with nodular graphite using different material models*. The 12th European Ls-Dyna Conference, Koblenz, 2019.

**Chuang Liu** born in 1990, is currently a lecturer at Nanjing University of Science and Technology, China. He received his PhD degree from Nanjing University of Science and Technology, China, in 2020. His main research interests is impact dynamics.



**Dongzhi Sun** born in 1953, is currently a researcher at *Fraunhofer Institute for Mechanics of Materials, Germany*. He received his PhD degree from *Institute of Ferrous Metallurgy of Aachen University, Germany*, in 1987. His main research interests include mechanisms and new methods for crash and production process simulations.

**Xianfeng Zhang** born in 1978, is currently a professor at *Nanjing University of Science and Technology, China*. He received his PhD degree from *Nanjing University of Science and Technology, China*, in 2005. His main research interests is impact dynamics.

**Florence Andrieux** born in 1967, is currently a researcher at *Fraunhofer Institute for Mechanics of Materials, Germany*. She received her PhD degree from *University of Technologie of Compiègne (UTC), France*, in 1991. Her main research interests include crash simulation accounting for manufacturing processes and forming and influence of strain hardening and damage.

**Tobias Gersterc** is currently a researcher at *Fraunhofer Institute for High Speed Dynamics, Ernst-Mach-Institute (EMI), Germany*. His main research interests is impact dynamics.